Stabilizing the Na/Beta-Al_2O_3 interface with mixed ionic-electronic conductor towards room-temperature solid-state sodium metal battery

Yao, Yiwei; Ma, Huirong; Yu, Xiaole; Wang, Xinxin; Chen, Jingjing; Lu, Liqiang; Wang, Dajian; Dong, Chenlong; Mao, Zhiyong

Published in:
Ceramics International

DOI:
10.1016/j.ceramint.2023.05.289

Document Version
Publisher's PDF, also known as Version of record

Publication date:
2023

Ceramics International 49 (2023) 27345–27351

Contents lists available at ScienceDirect

Ceramics International

journal homepage: www.elsevier.com/locate/ceramint

Stabilizing the Na/Beta-Al_2O_3 interface with mixed ionic-electronic conductor towards room-temperature solid-state sodium metal battery

Yiwei Yao [a,1], Huirong Ma [b,1], Xiaole Yu [a], Xinxin Wang [c], Jingjing Chen [d], Liqiang Lu [e], Dajian Wang [a], Chenlong Dong [a,f,**], Zhiyong Mao [b,*]

[a] Tianjin Key Laboratory for Photoelectric Materials and Devices, School of Materials Science and Engineering, Tianjin University of Technology, Tianjin, 300384, PR China
[b] Key Laboratory of Display Materials and Photoelectric Devices, Tianjin University of Technology, Ministry of Education, Tianjin, 300384, PR China
[c] Tianjin Lishen Battery Joint Stock Co. Ltd, Lishen Res. Inst, Tianjin, 300384, China
[d] Tianjin Key Laboratory of Quantum Optics and Intelligent Photonics, School of Science, Tianjin University of Technology, Tianjin, 300384, PR China
[e] Advanced Production Engineering, Engineering and Technology Institute Groningen, University of Groningen, Nijenborgh 4, 9747, AG, Groningen, the Netherlands
[f] State Key Laboratory of High Performance Ceramics and Superfine Microstructure, Shanghai Institute of Ceramics, Chinese Academy of Sciences, Shanghai, 200050, PR China

ARTICLE INFO

Handling Editor: Dr P. Vincenzini

Keywords:
Solid-state electrolyte
Mixed ionic-electronic conductive layer
Interface
Solid-state sodium metal battery

ABSTRACT

Beta-Al_2O_3, an inorganic solid electrolyte with high thermal stability and competitive ionic conductivity, is considered as the safe and efficient candidate for solid-state sodium metal batteries (SSMBs). The exhausting interfacial trouble between Beta-Al_2O_3 solid electrolyte and Na metal become the stumbling blocks of Beta-Al_2O_3 solid electrolyte applying at room-temperature. Herein, we demonstrate an efficient strategy by *in-situ* construction of mixed ionic-electronic (MIE) conductive layer (Na–Sn alloy and Na_2S) to engineer intimate Na/Beta-Al_2O_3-MIE interface *via* spontaneous conversion-alloying reaction between Na and SnS_2. Given by the modified MIE layer, the interfacial resistance is dramatically reduced from 3600 to 126 Ω cm^2. The Na symmetrical battery with a high critical current density of 0.9 mA cm^{-2} and it can stably cycle for 2650 h at 0.3 mA cm^{-2} with a low overpotential of 25 mV at room temperature. By incorporating ameliorative interface into SSMB, the $Na_3V_2(PO_4)_3$|Beta-Al_2O_3-MIE|Na harvests 103.6 mA h g^{-1} at 0.5 C after 250 cycles (97.4% capacity retention). This work rolled out an effective strategy for constructing stable Na/Beta-Al_2O_3 interface to realize room-temperature SSMBs.

1. Introduction

Solid-state sodium metal battery (SSMB), as a promising alternative to sodium-ion batteries, has proved its innate potential in stationary energy storage due to low cost, high safety and high energy density [1–3]. Among multitudinous inorganic solid-state electrolytes (SSEs) such as NASICON, Beta-Al_2O_3 and Na_3PS_4, Beta-Al_2O_3 electrolyte manifests superior ionic conductivity, low electronic conductivity, outstanding mechanical properties and (electro)chemical stability for SSMBs [4–8]. As a matter of that, Beta-Al_2O_3 electrolyte has applied as solid electrolytes for Na–S and ZEBRA batteries at high temperature (~300 °C) to decrease interface resistance between Beta-Al_2O_3 electrolyte and Na [9,10]. However, at room temperature, the high interfacial resistance hinders the Na^+ transfer at the interface and enhance the possibility of dendrite growth [6,11].

The presence of high interfacial resistance was related to poor Na wettability on Beta-Al_2O_3 electrolyte [12,13]. To facilitate Na/Beta-Al_2O_3 interface contact, sodium-inert Ni nanowire network [14], disordered carbon tubes [15], Pt mesh [16] coating were coated on the Beta-Al_2O_3 electrolyte surface, while these coating layers also requires high-temperature to realize the intimate contact with SSEs. Moreover, sodium-active Sn, Bi and Pb metals were alloyed with Na on Beta-Al_2O_3 by forming lower melting-point Na–Sn alloy [17], Na–Bi alloy [18,19], Na–Pb alloy [20], which filled the void of Na and consequently ensured

* Corresponding author.
** Corresponding author. Tianjin Key Laboratory for Photoelectric Materials and Devices, School of Materials Science and Engineering, Tianjin University of Technology, Tianjin, 300384, PR China.
E-mail addresses: dongchenlong@email.tjut.edu.cn (C. Dong), mzhy1984@163.com (Z. Mao).
[1] These authors contribute equally to this work.

https://doi.org/10.1016/j.ceramint.2023.05.289
Received 7 March 2023; Received in revised form 5 May 2023; Accepted 31 May 2023
Available online 1 June 2023

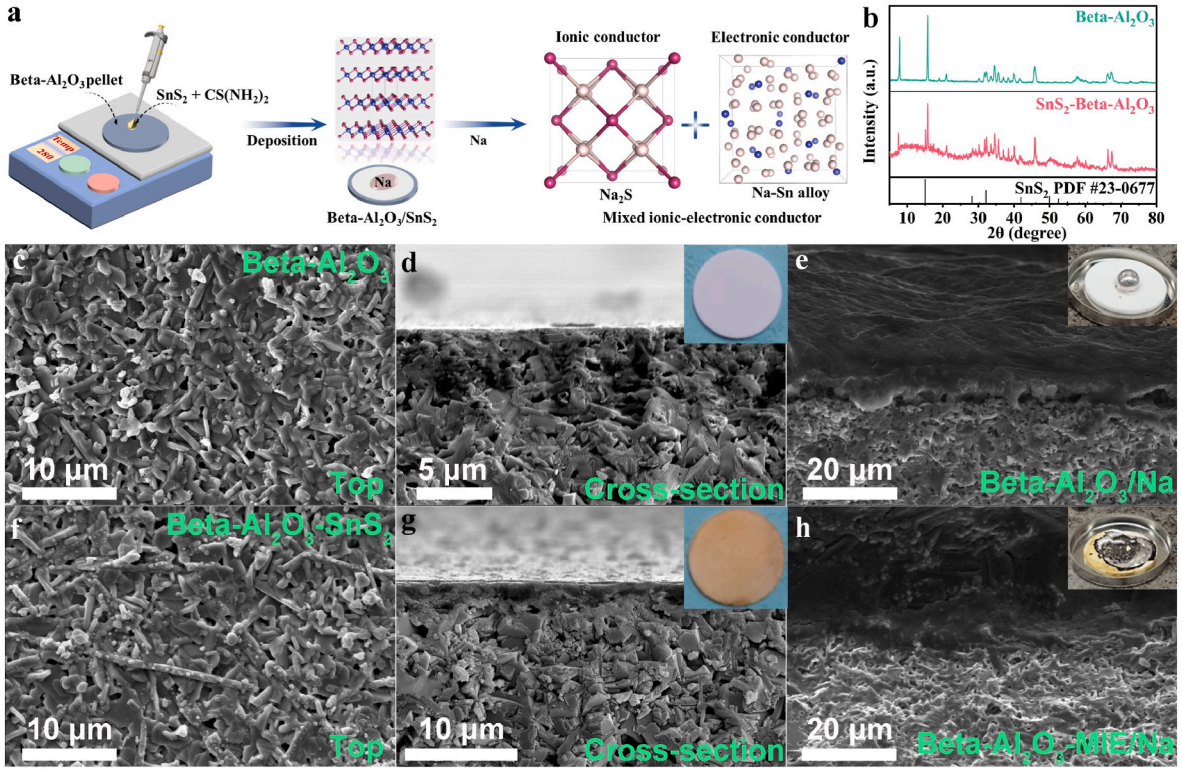

Fig. 1. Illustration of SnS_2 deposition on Beta-Al_2O_3 SSEs and corresponding characterizations of SSEs and Na/SSEs interface. (a) Schematic illustrations of thermal decomposition of SnS_2 on Beta-Al_2O_3 pellets and the construction of MIE layer. (b) XRD pattern of Beta-Al_2O_3 and SnS_2- Beta-Al_2O_3. (c) Top-view and (d) cross-section SEM images of Beta-Al_2O_3 pellet. Inset: digital photo of Beta-Al_2O_3 pellet. (e) The cross-section SEM images of Na/Beta-Al_2O_3 interface. Inset: wettability of molten Na on Beta-Al_2O_3 pellet. (f) Top-view and (g) cross-section SEM images of SnS_2-Beta-Al_2O_3 pellet. Inset: digital photo of SnS_2-Beta-Al_2O_3 pellet. (e) The cross-section SEM images of Na/Beta-Al_2O_3-MIE interface. Inset: wettability of molten Na on SnS_2-Beta-Al_2O_3 pellet.

a tight interfacial connection. Great efforts on Na/Beta-Al_2O_3 interface have been declared, yet it was still a long way to modify the interface composition and thereupon engineer stable room temperature SSMBs [3,5].

Theoretically, an intimate and stable Na/SSEs interface should provide the enough affinity with Na, reduce the nucleation barrier and simultaneously offers ionic transport pathway [21,22]. The interface layer with mixed ionic-electronic (MIE) conductive ability can achieve the aforementioned requirement, in which the ionic-conducting phase can homogenize the Na^+ transport and the electron-conducting phase can modify local current density to avoid inhomogeneous Na plating/stripping [23,24]. Such MIE layer can be engineered by the spontaneous reaction of Na metal with functional oxide (or sulfides) with conversion [25] (*eg.* $CuO + 2Na \rightarrow Cu + Na_2O$) or conversion-alloying (eg. $Sn(O,S)_2 + (x+4)Na \rightarrow Na_xSn + 2Na_2(O,S)$) mechanism [26,27].

Benefiting from the merits of MIE layer, a facial and viable strategy is executed to modify the Na/Beta-Al_2O_3 interface by introducing SnS_2 interlayer. Thereupon, by *in-situ* reaction of Na with SnS_2 at the Beta-Al_2O_3/Na interface, the MIE layer (Na–Sn alloy and Na_2S) is engineered to increase wettability and interfacial contact stability. Profiting from the conformal interface, the interfacial resistance reduces from 3600 Ω cm^2 (Na/Beta-Al_2O_3) to 126 Ω cm^2 (Na/Beta-Al_2O_3-MIE) and the critical current density of the Na symmetric batteries increases to 1.0 mA cm^{-2}. The Na|SnS_2-Beta-Al_2O_3-MIE|Na symmetrical battery can stably cycle for over 2650 h at 0.3 mA cm^{-2} (overpotential: <25 mV). Even at high current density of 0.6 mA cm^{-2}, the symmetrical battery can successfully operate for 100 h. When it served for solid-state sodium metal battery, $Na_3V_2(PO_4)_3$|Beta-Al_2O_3-MIE|Na delivers high ICE of 95.6% at 0.5 C and remains 97.4% capacity retention (103.6 mA h g^{-1}) after 250 cycles, thus breaking new ground for durable room-temperature solid-state sodium metal battery.

2. Experimental procedure

2.1. Sintering of Beta-Al_2O_3 solid-state electrolyte

Beta-Al_2O_3 solid electrolyte was synthesized by conventional solid sintering process from γ-AlOOH as the alumina source, Li_2CO_3 as the lithium source, and Na_2CO_3 as the sodium source [28,29]. The powder mixture with a stoichiometric composition ($Na_{1.67}Li_{0.33}Al_{10.67}O_{17}$) of Beta-$Al_2O_3$ was wet-milled with ethanol for 12 h using a planetary ball mill, and then sintered at 1250 °C for 2 h in a muffle furnace to obtain the precursor powder. The precursor powder was pressed into green pellets (Φ 12 mm). Finally, the green pellets covered with the precursor powder were calcined at 1450 °C for 2 h to obtain Beta-Al_2O_3 electrolyte.

2.2. Deposition of SnS_2 layer

1 mmol $SnCl_4{\cdot}5H_2O$ and 3 mmol CH_4N_2S were uniformly dissolved in 10 ml CH_3OH to prepare precursor solution. 5 μL precursor solution was dipped on Beta-Al_2O_3 pellets and the SnS_2 layer was deposited on Beta-Al_2O_3 pellets by thermal decomposition at 280 °C for 3 min.

2.3. Engineering of Na/Beta-Al_2O_3 and Na/Beta-Al_2O_3-MIE interfaces

The sodium foil was pressed by hand on Beta-Al_2O_3–SnS_2 and Beta-Al_2O_3 pellet to engineer Na/Beta-Al_2O_3 and Na/Beta-Al_2O_3-MIE interfaces.

2.4. Materials characterization

The phase compositions were identified by XRD diffractometer (ARL

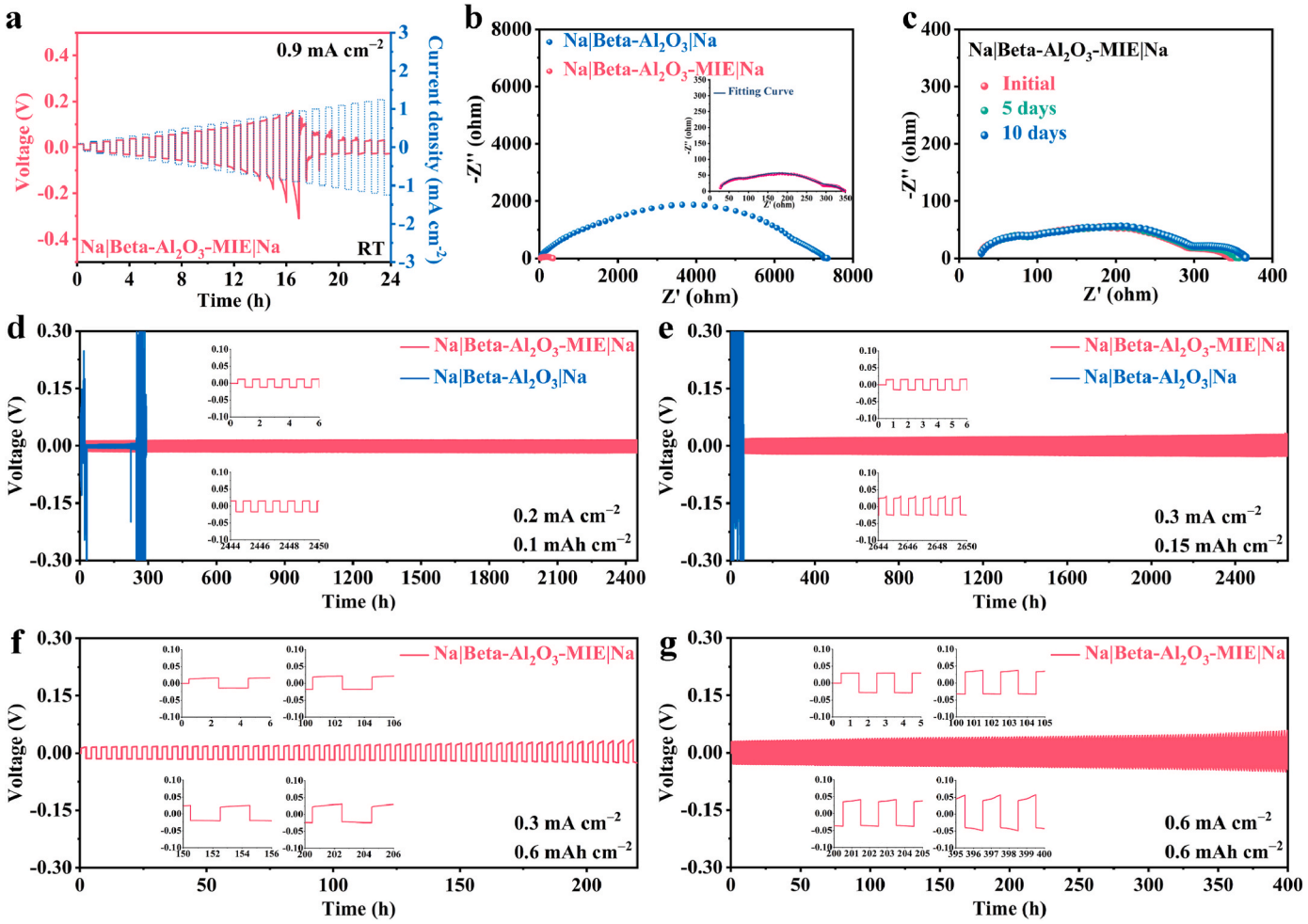

Fig. 2. Interface stability and electrochemical performance symmetreical battery. (a) Na plating/stripping profiles of Na|Beta-Al_2O_3-MIE|Na at step-increased current densities at room temperature. (b) The EIS data of the assembled Na|Beta-Al_2O_3-MIE|Na and Na|Beta-Al_2O_3|Na symmetrical batteries. (c) The EIS evolution of the Na|Beta-Al_2O_3-MIE|Na symmetrical battery during 10 days. Galvanostatic charging/discharging curves of Na|Beta-Al_2O_3-MIE|Na and Na|Beta-Al_2O_3|Na symmetrical batteries at current densities of (d) 0.2 mA cm^{-2} (areal capacity: 0.1 mA h cm^{-2}), (e) 0.3 mA cm^{-2} (areal capacity: 0.15 mA h cm^{-2}), (f) 0.3 mA cm^{-2} (areal capacity: 0.6 mA h cm^{-2}) and (g) 0.6 mA cm^{-2} (areal capacity: 0.6 mA h cm^{-2}) at room temperature.

Equinox 3000, France) equipped with Cu Kα radiation (λ = 0.15418 nm). A field emission scanning electron microscope (Quanta FEG, USA) equipped with energy-dispersive spectroscopy (EDS) equipment was employed to examine the morphology and elemental composition on surface and fractured cross-section of samples. For the preparation of cross-section SEM images, the Na/Beta-Al_2O_3 and Na/Beta-Al_2O_3-MIE were forced apart with the hands without further surface treatment and the samples are set in glovebox until SEM tests. The wettability was measured according to following process: putting a bit of Na on Beta-Al_2O_3 and SnS_2-Beta-Al_2O_3 pellets, then heating the Na/Beta-Al_2O_3 and Na/SnS_2-Beta-Al_2O_3 at 150 °C, and finally observing the wetting situation. XPS (Escalab 250 Xi, USA) measurement was performed to characterize MIE layer on Beta-Al_2O_3 pellet before and after cycling.

2.5. Electrochemical measurement

For symmetrical battery, the sodium foil with a diameter of 10 mm was pressed by hand on both sides of Beta-Al_2O_3–SnS_2 and Beta-Al_2O_3 pellet. Then, the Na symmetrical battery was assembled in the CR2032 coin cell. For assembling of solid-state sodium metal full battery, the CR2032 coin cell was fabricated in an argon-filled box with $Na_3V_2(PO_4)_3$, sodium foil, and Beta-Al_2O_3 pellet as the cathode, anode and electrolyte, respectively. $Na_3V_2(PO_4)_3$ cathode, acetylene black and polyvinylidene fluoride (PVDF) with a weight ratio of 8:1:1 was dispersed in N-methyl-2-pyrrolidone (NMP). The mixed slurry was ground for 30 min, ergo uniformly coated on Al foil and finally dried overnight. The mass loading of $Na_3V_2(PO_4)_3$ was *ca.* 1 mg cm^{-2}10 μL organic electrolyte of 1 M $NaClO_4$ in EC/DMC (1:1) with 5% FEC was dropped onto cathode to decrease the interfacial resistance between cathode and Beta-Al_2O_3 pellet. The ionic conductivity and interfacial resistance were measured by electrochemical impedance spectroscopy (EIS) on electrochemical workstation (CHI760E), in which the amplitude is 5 mV and the frequency ranges from 10^6 to 0.01 Hz. The critical current density (CCD), galvanostatic charge-discharge curve, cyclic stability and rate performance were measured on battery tester system (LAND CT2001A).

3. Results and discussion

3.1. Characterizations of Beta-Al_2O_3 and SnS_2-Beta-Al_2O_3

The Beta-Al_2O_3 pellet was synthesized by traditional high-temperature solid-state method. According to the stacking period of building block and chemical composition, the Beta-Al_2O_3 solid electrolyte has two kinds of crystal structures—hexagonal β-Al_2O_3 and rhombohedral β"-Al_2O_3 [6,30]. The XRD pattern of as-synthesized Beta-Al_2O_3 pellets show main characteristic peaks of β"-Al_2O_3 (PDF #84–1715) and trace amounts of β-Al_2O_3 (PDF #77–2312). The large number of Na^+

conducting planes and the high sodium content in conducting planes in β"-phase result in higher ionic conductivity than that of β-phase [30]. As a result, the ionic conductivity of Beta-Al_2O_3 solid electrolyte materials rose with the increase of β"-Al_2O_3 phase content. By calculation, the β″-phase content of Beta-Al_2O_3 pellet is as high as 93.4% (Fig. S1). The SnS_2 deposition on Beta-Al_2O_3 pellets was realized by thermal decomposition of $SnCl_4/CS(NH_2)_2$ solution (Fig. 1a) [31]. The XRD peak located at 14.5° for SnS_2-Beta-Al_2O_3 (Fig. 1b) can be indexed as the characteristic (001) plane of layered SnS_2 (PDF #23–0677). The digital photos of SnS_2-Beta-Al_2O_3 prove that a uniform SnS_2 coating layer can be constructed within 3 min (Fig. S2). Moreover, the SnS_2 coating layer is difficult to be removed, suggesting tight contact with Beta-Al_2O_3 electrolyte (Fig. S3).

The ionic conductivities of Beta-Al_2O_3 and SnS_2-Beta-Al_2O_3 pellets were measured by electrochemical impedance spectroscopy (EIS) at room temperature (Fig. S4). The total resistance (R_{total}) is equal to the sum of grain resistance (R_g) and grain boundary resistance (R_{gb}), and both of resistances are fitted by Zview software [32,33]. For Beta-Al_2O_3, the R_t value of Beta-Al_2O_3 pellet is 61.4 Ω at room temperature and the ionic conductivity is calculated to be 1.01×10^{-3} S cm^{-1}. Similarly, the ionic conductivity of SnS_2-Beta-Al_2O_3 is calculated to be 9.3×10^{-4} S cm^{-1} with the total resistance of 66 Ω at room temperature. The above results demonstrate that the SnS_2 coating layer has no significantly adverse effect on ionic conductivity of Beta-Al_2O_3 electrolyte.

3.2. Microstructural analyses of Na/Beta-Al_2O_3-MIE interface

The top-view (Fig. 1c) and cross-section SEM (Fig. 1d) images of Beta-Al_2O_3 pellets show abundant gaps and boundary valleys throughout the electrolyte pellets, which may be the destination of Na dendrite growth [2,34]. Thus, the design of interfacial composition between Na and Beta-Al_2O_3 to relieve poor solid-solid contact is required. After SnS_2 decomposition, plenty of SnS_2 particles tightly adhere to Beta-Al_2O_3 pellets (Fig. 1f and Fig. S5) and a thin SnS_2 layer with average thickness of *ca.* 230 nm is covered on Beta-Al_2O_3 pellet (Fig. 1g and Fig. S6). However, due to the relatively thin thickness and the low content of SnS_2 layer, the Sn and S dispersions are drifting (Fig. S7). The color of SnS_2-Beta-Al_2O_3 pellet changes into light coffee from white of Beta-Al_2O_3 pellet (inset of Fig. 1d and g). The element dispersive X-ray spectroscopy (EDX) spectrum of SnS_2-Beta-Al_2O_3 pellet displays that element of Sn and S were uniformly distributed. Furthermore, the wettability of molten Na on Beta-Al_2O_3 and SnS_2-Beta-Al_2O_3 pellets was investigated (inset of Fig. 1e and h). Conspicuously, the molten Na showed poor wettability on Beta-Al_2O_3 pellet. By contrast, the molten sodium can be spread out to form MIE layer due to the spontaneous reaction between Na and SnS_2 ($SnS_2 + (x+4)Na \rightarrow Na_xSn + 2Na_2S$), demonstrating the high wettability of Na on SnS_2-Beta-Al_2O_3 pellet [27,35]. Moreover, the MIE formation can be regard as the electrode reaction of typical SnS_2 anode for sodium ion battery (conversion: $SnS_2 + 4Na \rightarrow Sn + 2Na_2S$, alloying: $Sn + xNa \rightarrow Na_xSn$) [26,35,36]. Besides, it's obvious that there is huge gap at Na/Beta-Al_2O_3 interface, triggering poor interface contact and low tolerance of Na dendrite (Fig. 1e). While for Na/Beta-Al_2O_3-MIE, an intimate interface layer fills in the gap between Na and Beta-Al_2O_3 (Fig. 1h), suggesting the continuous Na^+ transport pathway. The thickness of MIE layer is speculated to be *ca.* 10 μm (Fig. S8).

3.3. Electrochemical performance of symmetrical batteries

To confirm the effects of MIE layer on interfacial resistance and stability, the symmetrical batteries of Na|Beta-Al_2O_3-MIE|Na and Na|Beta-Al_2O_3|Na were assembled by simple static pressure method. The critical current density (CCD) is used to estimate the Na plating/stripping ability under gradually increased current density [37,38]. For Na|Beta-Al_2O_3-MIE|Na, no sudden voltage drop can be observed until the current density increases into 0.9 mA cm^{-2}, which suggests the high inhibition ability of Na dendrites by MIE layer during cycles (Fig. 2a). While for Na|Beta-Al_2O_3|Na, the voltage suddenly decreases when current density increases into only 0.25 mA cm^{-2} as a result of continuous dendrites propagation and resultant short circuiting (Fig. S9). The asymmetry between stripping and plating observed at high current density is due to void formation during stripping and the rapid healing of the interface on plating, which has been confirmed in Beta-Al_2O_3 system [39].

The interface resistances have been determined by EIS plots, as shown in Fig. 2b. The first intercept can be ascribed to the bulk (R_{bulk}) and the first semicircle in high-frequency region corresponds to the grain boundary (R_g) of the Beta-Al_2O_3 electrolyte. The second and third semicircles in middle-frequency (R_{int1}) and low-frequency region (R_{int2}) are related to the MIE/Beta-Al_2O_3 and Na/MIE interfaces. The corresponded resistances have been fitted according to the following equivalent circuit diagram (Fig. S10). The R_{bulk}, R_{gb}, R_{int1} and R_{int2} are 24.47, 43.12, 220.2 and 61.17 Ω cm^2, respectively. Because the semicircle measured in the EIS consists of two interfaces between sodium and Beta-Al_2O_3, the fitted resistance is divided by two to obtain interface resistance of Na/Beta-Al_2O_3-MIE. The interface resistance of Na/Beta-Al_2O_3-MIE is calculated to be 126 Ω cm^2. Benefitting from the intimate interface, the interface resistance of Na/Beta-Al_2O_3-MIE (126 Ω cm^2) is much lower than that of Na/Beta-Al_2O_3 (~3600 Ω cm^2). Besides, the evolution interfacial resistance during rest for 20 days was monitored. Clearly, the EIS plots manifest negligible change within 10 days, proving the high stability of Na/Beta-Al_2O_3-MIE interface (Fig. 2c).

In order to investigate the cyclic stability of Na|Beta-Al_2O_3-MIE|Na and Na|Beta-Al_2O_3|Na symmetrical batteries, the galvanostatic charge/discharge in line with the ability of Na plating/stripping was measured. The Na|Beta-Al_2O_3-MIE|Na can steadily cycle at 0.2 mA cm^{-2} with an areal capacity of 0.1 mA h cm^{-2} for over 2450 h and provides a low overpotential of <15 mV (Fig. 2d). On the contrary, Na|Beta-Al_2O_3|Na battery shows fluctuations and irregular voltage changes even in the first few cycles. Unfortunately, a large overpotential can be observed in subsequent cycles and the battery short-circuits ultimately, because the sodium dendrites can easily penetrate into Beta-Al_2O_3 pellet at lower current density. Moreover, the EIS data for Na|Beta-Al_2O_3-MIE|Na during cycling at a current density of 0.2 mA cm^{-2} were tracked, where only little changes appear (Fig. S11). The cycling performance of Na|Beta-Al_2O_3-MIE|Na and Na|Beta-Al_2O_3|Na symmetric batteries were further measured at a current density of 0.3 mA cm^{-2} with an areal capacity of 0.15 mA h cm^{-2} at room temperature (Fig. 2e). Obviously, Na|Beta-Al_2O_3-MIE|Na symmetrical battery displays stable and low overpotentials of Na plating/stripping without drastic voltage disturbance during long cycling (overpotential: 18 mV at the 1st cycle and 25 mV at the 2650th cycle).

Moreover, the cyclic stability of Na|Beta-Al_2O_3-MIE|Na symmetrical battery with high areal capacity of 0.6 mA h cm^{-2} were investigated by two following measurement parameters: (1) current density: 0.3 mA cm^{-2}, plating/stripping time: 2 h and (2) current density: 0.6 mA cm^{-2}, plating/stripping time: 1 h. At a current density of 0.3 mA cm^{-2} with a plating/stripping time of 2 h, Na|Beta-Al_2O_3-MIE|Na battery presents low overpotentials of 18 mV at the 1st cycle and 27 mV at the 200th cycle (Fig. 2f). Even if the current density is as high as 0.6 mA cm^{-2} and the plating/stripping time is 1 h, the symmetrical battery can stably cycle for 400 h (overpotential: 29 mV at the 1st cycle and 53 mV at the 400th cycle).

3.4. Origin of enhanced interfacial stability

Due to the existence of voids and gaps between Na anode and Beta-Al_2O_3 electrolyte, the poor physical contact of Na/Beta-Al_2O_3 would induce the sluggish Na^+ transport and rapid dendrite growth. After introducing thin SnS_2 layer on Beta-Al_2O_3, the Na metal can spontaneously react with SnS_2 to form an intimate MIE interlayer, ergo fill in the gap between Na and Beta-Al_2O_3, and thus engineer continuous Na^+

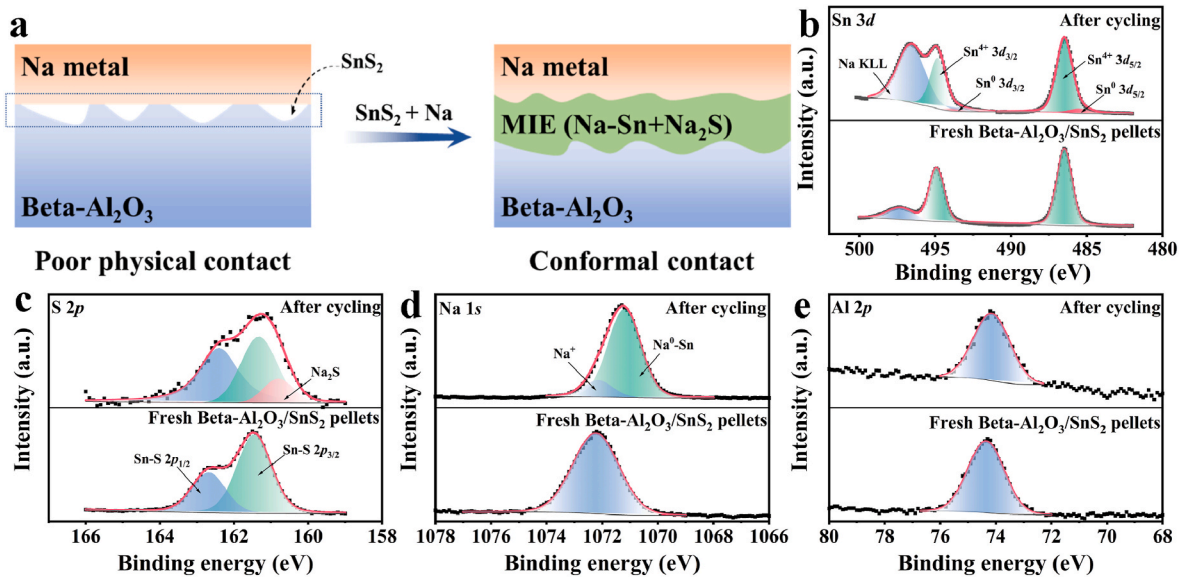

Fig. 3. The chemical environmental analysis of MIE layer before and after cycling. (a) Schematic of the mechanism of functional MIE layer between Na anode and Beta-Al_2O_3 electrolyte. High resolution XPS spectrum of (b) Sn 3*d*, (c) S 2*p*, (d) Na 1*s* and (e) Al 2*p* before and after cycling for 100 h at 0.2 mA cm^{-2}.

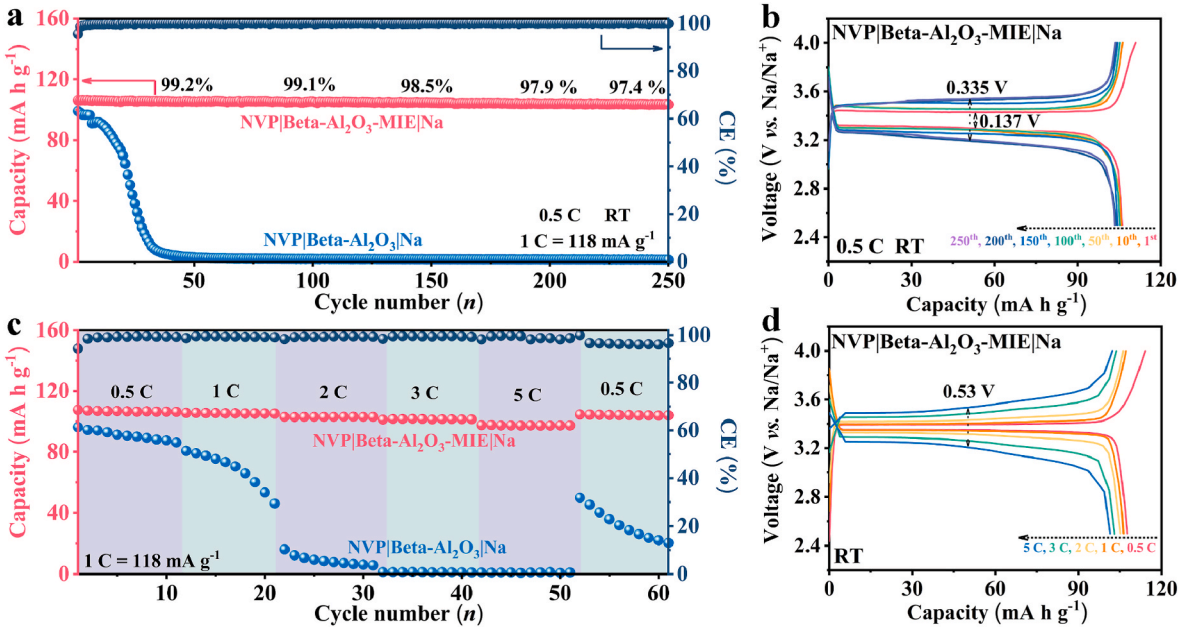

Fig. 4. Electrochemical performance of solid-state sodium full battery. (a) Cycling performance and (b) corresponding galvanostatic charging/discharging curves of $Na_3V_2(PO_4)_3$|Beta-Al_2O_3-MIE|Na battery at 0.5 C at room temperature. (c) Rate performance and (d) corresponding charging/discharging profiles of $Na_3V_2(PO_4)_3$|Beta-Al_2O_3-MIE|Na battery.

transport pathway (Fig. 3a). After cycling for 100 h at 0.2 mA cm^{-2}, the Na|Beta-Al_2O_3-MIE|Na symmetrical battery was separated (Fig. S12), and the contact region of Na anode and SnS_2 layer was black, suggesting the formation of MIE layer. To further analysis the reaction mechanism between SnS_2 layer and Na, the SnS_2-Beta-Al_2O_3 pellets before and after cycling were measured by X-ray photoelectron spectra (XPS). For Sn 3*d* spectrum (Fig. 3b), the peaks at 494.92 eV and 486.48 eV for SnS_2-Beta-Al_2O_3 pellets before and after cycling corresponds to Sn^{4+} $3d_{3/2}$ and Sn^{4+} $3d_{3/2}$, respectively [40]. The peak at 497.4 eV can be indexed as the Na KLL Auger line [41]. After cycling for 100 h, the new peaks located at 493.61 and 485.50 eV appear, which is attributed to Sn^0 $3d_{3/2}$ and Sn^0 $3d_{3/2}$, demonstrating the formation of Na–Sn alloy [42]. For S 2*p* spectrum (Fig. 3c), two strong peaks appear at 162.68 eV and 161.46 eV for SnS_2-Beta-Al_2O_3 pellets before and after cycling, which can be owned as the S^{2-} $2p_{1/2}$ and S^{2-} $2p_{3/2}$ from SnS_2 [43]. Additionally, a peak located at 160.8 eV emerges in recycled pellet, corresponding to ionic conductive Na_2S [43]. In viewing of Na 1*s* spectrum (Fig. 3d), the peak at 1072.15 eV corresponds to Na^+ in Beta-Al_2O_3 electrolyte. However, a strong peak at 1071.21 eV emerges in recycled pellets, and it can be Na^0 in Na–Sn alloy [44]. While for Al 2*p* spectrum (Fig. 3e), there is no obvious peak shift and extra Al^0 peak observed, confirming the remarkable electro(chemical) stability [45]. Therefore, the formation of electronic-conducting Na–Sn alloy can improve the wettability of Na on solid electrolyte, promote the conformal contact and relieve the Na penetration into electrolyte, while the ionic-conducting Na_2S can homogenize the Na^+ transport.

3.5. Electrochemical performance of solid-state sodium-metal batteries

To verify the possibility of practical application, taking three-dimensional $Na_3V_2(PO_4)_3$ (donated as NVP) as cathode, the NVP|Beta-Al_2O_3-MIE|Na and NVP|Beta-Al_2O_3|Na full battery were assembled. The theoretical capacity of $Na_3V_2(PO_4)_3$ is 118 mA h g^{-1} based on V^{4+}/V^{3+} (1 C = 118 mA g^{-1}). As shown in Fig. 4a, the initial discharge capacity of NVP|Beta-Al_2O_3-MIE|Na is 106.1 mA h g^{-1} at 0.5 C with an ICE of 95.6%. Reassuring that, it offers a reversible capacity of 103.3 mA h g^{-1} after 250 cycles, corresponding to capacity retention of 97.4% at room temperature. The NVP|Beta-Al_2O_3-MIE|Na battery shows a maximum energy density of 349 Wh kg^{-1} (discharge medium voltage: 3.29 V, 1st discharge capacity: 106.1 mA h g^{-1}) at 0.5 C, as shown in Fig. 4b. Such highly overlapped charge/discharge curves and small potential polarization further confirm the high stability of Na/Beta-Al_2O_3-MIE interface. While for NVP|Beta-Al_2O_3|Na, it harvests a low discharge capacity of 99.1 mA h g^{-1} at the 1st cycle and comes through rapid capacity decay after ten cycles.

Besides, the discharge capacity of NVP|Beta-Al_2O_3-MIE|Na at 0.5 C, 1 C, 2 C, 3 C and 5 C was 106.3, 105.4, 103.0, 101.3 and 97.6 mA h g^{-1}, respectively (Fig. 4c). When the rate returns to 0.5 C, the specific capacity recovered to 104.2 mA h g^{-1}, demonstrating that the rapid Na^+ transport in MIE layer. According to the charge/discharge curves of 5 C, NVP|Beta-Al_2O_3-MIE|Na battery can provide a high capacity of 97.6 mA h g^{-1} and high discharge potential of 3.20 V (Fig. 4d). In contrast, the performance of NVP|Beta-Al_2O_3|Na suffers from rapid capacity attenuation at high rates. Such results prove that the MIE layer composed of electronic-conducting Na–Sn alloy and ionic-conducting Na_2S can extremely optimize the interfacial stability and Na^+ transport pathway.

4. Conclusion

In summary, SnS_2 interlayer was decorated on Beta-Al_2O_3 pellet by thermal deposition to engineer intimate Na/Beta-Al_2O_3 interface. During connecting with Na metal anode, SnS_2 spontaneously reacts with Na to form mixed ionic-electronic conductor, which is comprised of electronic-conducting Na–Sn alloy and ionic-conducting Na_2S. The MIE layer can provide a continuous and tight interface between Beta-Al_2O_3 and Na, which facilitates the uniform and rapid Na^+ transfer and thus engineer a stable interface for rapid Na plating/stripping. Such MIE interlayer fills in the gaps and holes of Na/Beta-Al_2O_3, resulting in decreased interfacial resistance from 3600 to 126 Ω cm^2 and enhanced critical current density from 0.25 to 0.90 mA cm^{-2}. Benefitting the conformal interface, the NVP|Beta-Al_2O_3-MIE|Na symmetric battery can operate stably for 2650 h at 0.3 mA cm^{-2} with an overpotential of <25 mV. This work may pave new pathway to solve the poor physical contact of Na/Beta-Al_2O_3 interface and promote the development of the next-generation room-temperature SSMBs.

Declaration of competing interest

The authors declare that they have no known competing financial interests or personal relationships that could have appeared to influence the work reported in this paper.

Acknowledgment

This work was supported by the National Natural Science Foundation of China (Grant No. 52202282), Opening Project of State Key Laboratory of High Performance Ceramics and Superfine Microstructure (Grant No. SKL202209SIC) and Natural Science Foundation of Tianjin City (Grant No. 22JCYBJC00040).

Appendix A. Supplementary data

Supplementary data to this article can be found online at https://doi.org/10.1016/j.ceramint.2023.05.289.

References

[1] J. Deng, W.-B. Luo, S.-L. Chou, H.-K. Liu, S.-X. Dou, Sodium-ion batteries: from academic research to practical commercialization, Adv. Energy Mater. 8 (2018), 1701428.
[2] B. Lee, E. Paek, D. Mitlin, S.W. Lee, Sodium metal anodes: emerging solutions to dendrite growth, Chem. Rev. 119 (2019) 5416–5460.
[3] Y. Wang, Y. Wang, Y.-X. Wang, X. Feng, W. Chen, X. Ai, H. Yang, Y. Cao, Developments and perspectives on emerging high-energy-density sodium-metal batteries, Chem 5 (2019) 2547–2570.
[4] J.-J. Kim, K. Yoon, I. Park, K. Kang, Progress in the development of sodium-ion solid electrolytes, Small Methods 1 (2017), 1700219.
[5] W. Hou, X. Guo, X. Shen, K. Amine, H. Yu, J. Lu, Solid electrolytes and interfaces in all-solid-state sodium batteries: progress and perspective, Nano Energy 52 (2018) 279–291.
[6] Y. Lu, L. Li, Q. Zhang, Z. Niu, J. Chen, Electrolyte and interface engineering for solid-state sodium batteries, Joule 2 (2018) 1747–1770.
[7] Q. Lu, A. Yang, A. Omar, Q. Ma, F. Tietz, O. Guillon, D. Mikhailova, Recent advances in stabilization of sodium metal anode in contact with organic liquid and solid-state electrolytes, Energ. Tech. 10 (2022), 2200149.
[8] H. Su, S.-W. Zhang, Y.-M. Liu, C. Yang, L.-X. Zhang, S. Xin, Y. You, $Na_3Zr_2Si_2PO_{12}$ solid-state electrolyte with glass-like morphology for enhanced dendrite suppression, Rare Met. 41 (2022) 4086–4093.
[9] K.B. Hueso, M. Armand, T. Rojo, High temperature sodium batteries: status, challenges and future trends, Energy Environ. Sci. 6 (2013) 734–749.
[10] Y. Wang, D. Zhou, V. Palomares, D. Shanmukaraj, B. Sun, X. Tang, C. Wang, M. Armand, T. Rojo, G. Wang, Revitalising sodium–sulfur batteries for non-high-temperature operation: a crucial review, Energy Environ. Sci. 13 (2020) 3848–3879.
[11] Q. Zhao, S. Stalin, L.A. Archer, Stabilizing metal battery anodes through the design of solid electrolyte interphases, Joule 5 (2021) 1119–1142.
[12] J. Kasemchainan, S. Zekoll, D. Spencer Jolly, Z. Ning, G.O. Hartley, J. Marrow, P. G. Bruce, Critical stripping current leads to dendrite formation on plating in lithium anode solid electrolyte cells, Nat. Mater. 18 (2019) 1105–1111.
[13] S.-H. Wang, J. Yue, W. Dong, T.-T. Zuo, J.-Y. Li, X. Liu, X.-D. Zhang, L. Liu, J.-L. Shi, Y.-X. Yin, Y.-G. Guo, Tuning wettability of molten lithium *via* a chemical strategy for lithium metal anodes, Nat. Commun. 10 (2019) 4930.
[14] Y. Hu, Z. Wen, X. Wu, Y. Lu, Nickel nanowire network coating to alleviate interfacial polarization for Na-beta battery applications, J. Power Sources 240 (2013) 786–795.
[15] T. Wu, Z. Wen, C. Sun, X. Wu, S. Zhang, J. Yang, Disordered carbon tubes based on cotton cloth for modulating interface impedance in β″-Al_2O_3-based solid-state sodium metal batteries, J. Mater. Chem. 6 (2018) 12623–12629.
[16] G. Li, X. Lu, J.Y. Kim, J.P. Lemmon, V.L. Sprenkle, Improved cycling behavior of ZEBRA battery operated at intermediate temperature of 175 °C, J. Power Sources 249 (2014) 414–417.
[17] D. Reed, G. Coffey, E. Mast, N. Canfield, J. Mansurov, X. Lu, V. Sprenkle, Wetting of sodium on β″-Al_2O_3/YSZ composites for low temperature planar sodium-metal halide batteries, J. Power Sources 227 (2013) 94–100.
[18] D. Jin, S. Choi, W. Jang, A. Soon, J. Kim, H. Moon, W. Lee, Y. Lee, S. Son, Y.-C. Park, H. Chang, G. Li, K. Jung, W. Shim, Bismuth islands for low-temperature sodium-Beta alumina batteries, ACS Appl. Mater. Interfaces 11 (2019) 2917–2924.
[19] K. Ahlbrecht, C. Bucharsky, M. Holzapfel, J. Tübke, M.J. Hoffmann, Investigation of the wetting behavior of Na and Na alloys on uncoated and coated Na-β”-alumina at temperatures below 150 °C, Ionics 23 (2017) 1319–1327.
[20] H.-J. Chang, X. Lu, J.F. Bonnett, N.L. Canfield, K. Han, M.H. Engelhard, K. Jung, V. L. Sprenkle, G. Li, Decorating β″-alumina solid-state electrolytes with micron Pb spherical particles for improving Na wettability at lower temperatures, J. Mater. Chem. 6 (2018) 19703–19711.
[21] M. Bai, Y. Liu, K. Zhang, X. Tang, S. Liu, Y. Ma, Alloying-triggered heterogeneous nucleation for the flexible sodium metallic batteries, Energy Storage Mater. 38 (2021) 499–508.
[22] H. Wang, E. Matios, J. Luo, W. Li, Combining theories and experiments to understand the sodium nucleation behavior towards safe sodium metal batteries, Chem. Soc. Rev. 49 (2020) 3783–3805.
[23] B. Tang, P.W. Jaschin, X. Li, S.-H. Bo, Z. Zhou, Critical interface between inorganic solid-state electrolyte and sodium metal, Mater. Today 41 (2020) 200–218.
[24] K. Lin, X. Xu, X. Qin, J. Wu, Q. Liu, Z. Tang, S. He, Y. Ye, F. Kang, B. Li, In situ constructed ionic-electronic dual-conducting scaffold with reinforced interface for high-performance sodium metal anodes, Small 17 (2021), 2104021.
[25] R. Miao, C. Wang, D. Li, C. Sun, J. Li, H. Jin, Uniform Na metal plating/tripping design for highly reversible solid-state Na metal batteries at room temperature, Small 18 (2022), 2204487.
[26] Z. Liu, A. Daali, G.-L. Xu, M. Zhuang, X. Zuo, C.-J. Sun, Y. Liu, Y. Cai, M.D. Hossain, H. Liu, K. Amine, Z. Luo, Highly reversible sodiation/desodiation from a carbon-sandwiched SnS_2 nanosheet anode for sodium ion batteries, Nano Lett. 20 (2020) 3844–3851.
[27] X. Wang, J. Chen, Z. Mao, D. Wang, In situ construction of a stable interface induced by the SnS_2 ultra-thin layer for dendrite restriction in a solid-state sodium metal battery, J. Mater. Chem. 9 (2021) 16039–16045.
[28] Y. Yao, X. Wang, C. Dong, J. Chen, D. Wang, Z. Mao, Constructing effective interface for room-temperature Beta-Al_2O_3 based sodium metal batteries, J. Power Sources 523 (2022), 231034.

[29] H. Ma, H. Zhao, Y. Song, S. Liu, Z. Mao, D. Wang, Metastable polymorphs and luminescence of boehmite-derived alumina doped with divalent europium ions, Funct. Mater. Lett. 15 (2022), 2251023.
[30] D.-H. Lee, S.-T. Lee, J.-S. Kim, S.-K. Lim, Analysis of properties of partially stabilized zirconia-doped Na^{+}-beta-alumina prepared by calcining-cum-sintering process, Mater. Res. Bull. 96 (2017) 143–148.
[31] Z. Hadef, K. Kamli, A. Attaf, M.S. Aida, B. Chouial, Effect of $SnCl_2$ and $SnCl_4$ precursors on SnS_x thin films prepared by ultrasonic spray pyrolysis, J. Semiconduct. 38 (2017), 063001.
[32] C. Wang, H. Jin, Y. Zhao, Surface potential regulation realizing stable sodium/$Na_3Zr_2Si_2PO_{12}$ interface for room-temperature sodium metal batteries, Small 17 (2021), 2100974.
[33] Y. Lu, J.A. Alonso, Q. Yi, L. Lu, Z.L. Wang, C. Sun, A high-performance monolithic solid-state sodium battery with Ca^{2+} Doped $Na_3Zr_2Si_2PO_{12}$ electrolyte, Adv. Energy Mater. 9 (2019), 1901205.
[34] Q.-Y. Yang, Z. Yu, Y. Li, W. Zhang, H.-W. Yuan, H.-J. Li, W. Ma, S.-M. Zhu, S. Li, Understanding and modifications on lithium deposition in lithium metal batteries, Rare Met. 41 (2022) 2800–2818.
[35] B. Qu, C. Ma, G. Ji, C. Xu, J. Xu, Y.S. Meng, T. Wang, J.Y. Lee, Layered SnS_2-reduced graphene oxide composite – a high-capacity, high-rate, and long-cycle Life sodium-ion battery anode material, Adv. Mater. 26 (2014) 3854–3859.
[36] S. Li, Z. Zhao, C. Li, Z. Liu, D. Li, SnS_2@C Hollow nanospheres with robust structural stability as high-performance anodes for sodium ion batteries, Nano-Micro Lett. 11 (2019) 14.
[37] R.J.Y. Park, C.M. Eschler, C.D. Fincher, A.F. Badel, P. Guan, M. Pharr, B. W. Sheldon, W.C. Carter, V. Viswanathan, Y.-M. Chiang, Semi-solid alkali metal electrodes enabling high critical current densities in solid electrolyte batteries, Nat. Energy 6 (2021) 314–322.
[38] Y. Lu, C.-Z. Zhao, H. Yuan, X.-B. Cheng, J.-Q. Huang, Q. Zhang, Critical current density in solid-state lithium metal batteries: mechanism, influences, and strategies, Adv. Funct. Mater. 31 (2021), 2009925.
[39] D.S. Jolly, Z. Ning, J.E. Darnbrough, J. Kasemchainan, G.O. Hartley, P. Adamson, D.E.J. Armstrong, J. Marrow, P.G. Bruce, Sodium/Na β'' alumina interface: effect of pressure on voids, ACS Appl. Mater. Interfaces 12 (2020) 678–685.
[40] T.J. Whittles, L.A. Burton, J.M. Skelton, A. Walsh, T.D. Veal, V.R. Dhanak, Band alignments, valence bands, and core levels in the tin sulfides SnS, SnS_2, and Sn_2S_3: experiment and theory, Chem. Mater. 28 (2016) 3718–3726.
[41] A. Kikas, E. Nõmmiste, R. Ruus, A. Saar, I. Martinson, Na K Photoabsorption and resonant KLL auger spectra in NaF and NaCl, Surf. Rev. Lett. 9 (2002) 1303–1308.
[42] X. Zheng, H. Fu, C. Hu, H. Xu, Y. Huang, J. Wen, H. Sun, W. Luo, Y. Huang, Toward a stable sodium metal anode in carbonate electrolyte: a compact, inorganic alloy interface, J. Phys. Chem. Lett. 10 (2019) 707–714.
[43] Y. Hu, B. Luo, D. Ye, X. Zhu, M. Lyu, L. Wang, An innovative freeze-dried reduced graphene oxide supported SnS_2 cathode active material for aluminum-ion batteries, Adv. Mater. 29 (2017), 1606132.
[44] X. Yu, A. Manthiram, Na_2S–carbon nanotube fabric electrodes for room-temperature sodium–sulfur batteries, Chem. Eur J. 21 (2015) 4233–4237.
[45] T. Tago, N. Kataoka, H. Tanaka, K. Kinoshita, S. Kishida, XPS study from a clean surface of Al_2O_3 single crystals, Process Eng. 216 (2017) 175–181.